Optimizing symmetry-based recoupling sequences in solid-state NMR by pulse-transient compensation and asynchronous implementation

Author(s):
Hellwagner, Johannes; Sharma, Kshama; Tan, Kong O.; Wittmann, Johannes J.; Meier, Beat H.; Madhu, Perunthiruthy K.; Ernst, Matthias

Publication date:
2017-06-27

Permanent link:
https://doi.org/10.3929/ethz-b-000190899

Originally published in:
The Journal of Chemical Physics 146(24), https://doi.org/10.1063/1.4989542

Funding acknowledgement:
146757 - NMR studies in the Solid State (SNF)

Optimizing symmetry-based recoupling sequences in solid-state NMR by pulse-transient compensation and asynchronous implementation

Johannes Hellwagner,[1] Kshama Sharma,[2] Kong Ooi Tan,[1] Johannes J. Wittmann,[1] Beat H. Meier,[1,*] P.K. Madhu,[2,3,*] Matthias Ernst[1,*]

[1] Physical Chemistry, ETH Zurich, Vladimir-Prelog-Weg 2, 8093 Zurich, Switzerland

[2] TIFR Centre for Interdisciplinary Sciences, 21 Brundavan Colony, Narsingi, Hyderabad 500075, India

[3] Department of Chemical Sciences, Tata Institute of Fundamental Research, Homi Bhabha Road, Colaba, Mumbai 400005, India

*Corresponding authors: Matthias Ernst (maer@ethz.ch)

P.K. Madhu (madhu@tifr.res.in)

Beat H. Meier (beme@ethz.ch)

Abstract

Pulse imperfections like pulse transients and radio-frequency field maladjustment or inhomogeneity are the main sources of performance degradation and limited reproducibility in solid-state NMR experiments. We quantitatively analyze the influence of such imperfections on the performance of symmetry-based pulse sequences and describe how they can be compensated. Based on a triple-mode Floquet analysis, we develop a theoretical description of symmetry-based dipolar recoupling sequences, in particular $\mathrm{R26}_4^{11}$, calculating first- and second-order effective Hamiltonians using real pulse shapes. We discuss the various origins of effective fields, namely pulse transients, deviation from the ideal flip angle, and fictitious fields, and develop strategies to counteract them for the restoration of full transfer efficiency. We compare experimental applications of transient-compensated pulses and an asynchronous implementation of the sequence to a super cycle, SR26, which is known to be efficient in compensating higher-order error terms. We are able to show the superiority of R26 compared to the super cycle, SR26, given the ability to reduce experimental error on the pulse sequence by pulse-transient compensation and a complete theoretical understanding of the sequence.

This manuscript was accepted by J. Chem. Phys. Click here to see the version of record.

Introduction

Solid-state nuclear magnetic resonance (NMR) spectroscopy relies on magic-angle spinning (MAS) to increase the resolution and sensitivity by averaging anisotropic interactions. To reintroduce such interactions, which contain structural information, one often applies radio-frequency (rf) pulse sequences to interfere with the averaging by MAS. The dipolar coupling, in particular, contains direct and valuable structure information because the dipolar coupling constant scales with the inverse cube of the internuclear distance.[1,2] A large number of dipolar recoupling sequences exist for the determination of dipolar couplings under MAS.[3–6] These methods give information on qualitative internuclear proximity and, in some cases, quantitative distance restraints. In addition, dipolar-recoupling sequences allow the excitation of multiple-quantum coherences, providing information on torsion angles.[7,8]

Symmetry-based dipolar-recoupling sequences (so called $\mathrm{C}N_n^\nu$ and $\mathrm{R}N_n^\nu$ sequences)[9] allow for a selective recoupling of certain terms in the dipolar Hamiltonian and have been used to determine distances up to a 5 Å for isolated ^{13}C-^{13}C spin pairs.[10] Important properties of these sequences are γ encoding and robustness towards pulse error terms and rf inhomogeneity.[9] The property of γ encoding implies that the first-order effective Hamiltonian is only phase modulated by the third Euler angle with respect to the laboratory frame, γ. This leads to high double-quantum recoupling efficiencies with a theoretical maximum of 73% for the first transient. In practice, such a high efficiency is usually unachievable, due to higher-order error terms contributing to the Hamiltonian and experimental artefacts including pulse imperfections due to pulse transients.[11]

Pulse transients are a consequence of the finite bandwidth of the resonance circuit in the probe as well as an impedance mismatch of the electrical components in the experimental setup. In practice, significant deviations between the ideal pulses, usually programmed as square pulses, and the actual B_1 field are observed. These deviations are most prominent at points where sudden changes of the amplitude or the phase of the rf pulse happen, as is required for symmetry-based sequences. Several analytical models to describe transients

This manuscript was accepted by J. Chem. Phys. Click here to see the version of record.

have been proposed in the literature. They are characterized by a time constant for the finite build-up time, τ_{rise}, and an "electronic" offset frequency, ω_{off}.[11] The deviation of the rising edge of an isolated, ideal pulse is described by Eq. (1), following the model in Ref. [11].

$$p(t) = p_{\mathrm{ideal}}(t) * \left(1 - \exp\left(-\frac{t}{\tau_{\mathrm{rise}}}\right) * \exp(i\omega_{\mathrm{off}}t)\right) \quad (1)$$

In linear approximation, the deviations for back-to-back pulses are modelled as a superposition of the rising and trailing pulse transients of the two pulses. The pulse transients are known to affect the spin trajectories and introduce additional effective fields in the Floquet picture leading to a distortion of the effective rotation axes, and ultimately, resulting in a significant loss in transfer efficiency. In phase-modulated recoupling sequences like the R and C sequences, the biggest effect comes from the effective fields that cause a mismatch of the resonance condition between the spin rotation and the sample rotation.[12]

Restoring the transfer efficiency requires the compensation of the effective fields generated by pulse transients. Several strategies have been proposed focusing on minimizing those effective fields. These include special tune-up sequences,[13,14] tunable LC circuits,[15] modification of the pulse sequence,[16] or transient compensation of the pulses based on linear-response theory.[12,17–19]

A different, experimentally simpler, compensation of effective fields involves the use of super-cycled pulse sequences.[20,21] It is known that phase cycling a pulse sequence can eliminate some higher-order terms and, therefore, reduces the magnitude of these effective fields and increases the dipolar recoupling efficiency.

In this work, we focus on the symmetry-based double-quantum recoupling sequence $\mathrm{R26}_4^{11}$ as a model for the symmetry-based sequences and its super-cycled version, denoted as SR26 (Figure 1A). It is well known that the super-cycled sequence is more stable and leads to more reproducible results at the cost of a loss of γ encoding, and hence, a decrease of the theoretical transfer efficiency from 73% to 52%. Based on a tri-modal Floquet description we show that a first-order analysis of the Hamiltonian is insufficient for a full theoretical

This manuscript was accepted by J. Chem. Phys. Click here to see the version of record.

understanding due to the magnitude of the second-order error terms.[22] We extend the theoretical description[21] to an analysis of the influence of the CSA-CSA cross terms. We adapt the concepts for the asynchronous implementation of symmetry-based pulse sequences, recently reported for the POST-C7 sequence, to minimize to second-order terms.[23,24] Furthermore, we investigate the influence of pulse transients on the sequence and show the effect of transient compensation.

We compare the different ways to compensate the effective fields and discuss advantages and disadvantages of them. We show that concepts developed earlier for C-type sequences can be extended to R-type sequences.

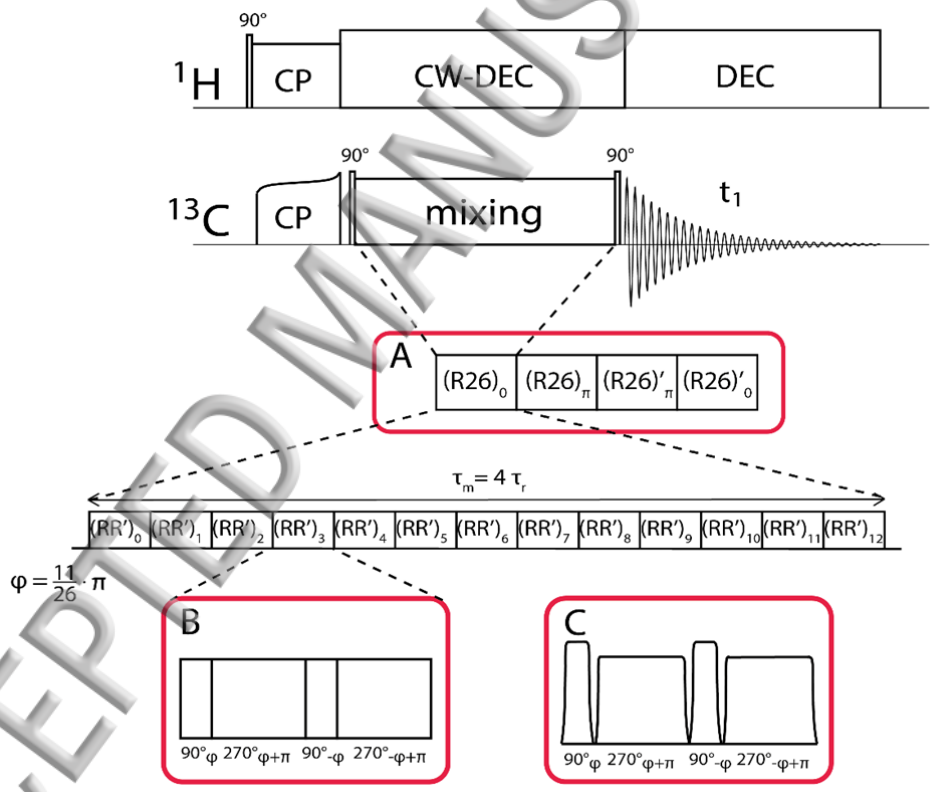

Figure 1: Schematic representation of the dipolar double-quantum R26-recoupling sequence in a 1D experiment. Various implementations are shown with one example as a supercycle SR26 (A) with permutation and π-phase shift of the R26 mixing block. The dash symbolizes a phase permutation. Different basic R-elements are used to make up the R26 mixing block: (B) R-element consisting of

ideal rectangular pulses with composition $(\pi/2)_{\varphi}(3\pi/2)_{\varphi+\pi}$. (C) Transient compensated R element consisting of amplitude-shaped pulses with sine-shaped edges.

Theory

The symmetry-based RN_n^{ν} sequences are generated from a basic element R_{φ} that implements a π rotation about an axis in the x-y plane.[9] The most widely used implementations are either a simple $(\pi)_{\varphi}$ pulse or a composite pulse $(\pi/2)_{\varphi}(3\pi/2)_{\varphi+\pi}$ both corresponding to a net π rotation. For the complete sequence, $N/2$ $R_{\varphi}R_{-\varphi}$ elements are fit into *n* rotor periods with the phase φ given as $\pi\nu/N$. The correct selection of symmetry coefficients *N, n,* and ν allows for a selective recoupling or decoupling of specific interactions based on the rotational properties of their spatial and spin components. A theoretical description of these types of sequences is either based on symmetry arguments and average-Hamiltonian theory,[25] or bi-modal Floquet theory.[26–28] The relevant frequencies are the MAS frequency ω_{r}, and the modulation frequency of the pulse sequence ω_{m}. In the bi-modal Floquet description, we assume that the R element corresponds to an ideal inversion propagator. In reality, however, a more generalized description has to be applied since pulse imperfections in the form of rf-field amplitude missetting or inhomogeneity, or phase transients can lead to a deviation from the perfect inversion properties of the R element. As a consequence of this, the rf trajectory will no longer be cyclic and the Floquet description has to be extended with a third frequency, namely the effective field ω_{eff}.[29]

For the theoretical description of RN_n^{ν}, we assume an ideal homonuclear-coupled two-spin system (*p* = 1, 2) with chemical-shift interactions. In spherical-tensor notation the rotating-frame Hamiltonian is given by

$$\mathcal{H}(t) = \sum_{p=1}^{2} \omega_p(t) T_{1,0}^{(p)} + \omega_{1,2}(t) T_{2,0}^{(1,2)} + \mathcal{H}_{\mathrm{rf}}(t) \qquad (2)$$

with an arbitrary amplitude- and phase-modulated rf-field Hamiltonian

This manuscript was accepted by J. Chem. Phys. Click here to see the version of record.

$$\mathcal{H}_{\mathrm{rf}}(t) = \omega_1(t) \sum_p (\cos(\varphi(t)) S_{px} + \sin(\varphi(t)) S_{py}). \tag{3}$$

Here, $\omega_p(t)$ represents the time-dependent chemical shift of spin p, $\omega_{1,2}(t)$ the dipolar coupling, and $\omega_1(t)$ and $\varphi(t)$ the amplitude and the phase of an arbitrary pulse sequence, respectively. The Floquet analysis is done in an interaction frame of the rf-field Hamiltonian. The interaction-frame transformation is defined by the propagator

$$\hat{U}_{\mathrm{rf}}(t) = \hat{T} \exp\left(-i \int_0^t \mathcal{H}_{\mathrm{rf}}(t')dt'\right) \tag{4}$$

with the interaction-frame Hamiltonian given by

$$\tilde{\mathcal{H}}(t) = \hat{U}_{\mathrm{rf}}^{-1}(t) \mathcal{H}(t) \hat{U}_{\mathrm{rf}}(t) . \tag{5}$$

Here, $\hat{T}$ represents the Dyson time-ordering operator.[30] In the general case of a tri-modal Floquet description with $\omega_{\mathrm{eff}} \neq 0$, the interaction-frame Hamiltonian can be written as a Fourier series

$$\tilde{\mathcal{H}}(t) = \sum_{n=-2}^{2} \sum_{k=-\infty}^{\infty} \sum_{\ell=-2}^{2} \tilde{\mathcal{H}}^{(n,k,\ell)} e^{in\omega_{\mathrm{r}}t} e^{ik\omega_{\mathrm{m}}t} e^{i\ell\omega_{\mathrm{eff}}t} \tag{6}$$

with the Fourier coefficients $\tilde{\mathcal{H}}^{(n,k,\ell)}$ given by

$$\tilde{\mathcal{H}}^{(0,k,\ell)} = \sum_{p=1}^{2} \omega_p^{(0)} \sum_{s=-1}^{1} a_{1,s}^{(k,\ell)} T_{1,s}^{(p)} \tag{7}$$

$$\tilde{\mathcal{H}}^{(n,k,\ell)} = \omega_{1,2}^{(n)} \sum_{s=-2}^{2} a_{2,s}^{(k,\ell)} T_{2,s}^{(1,2)} + \sum_{p=1}^{2} \omega_p^{(n)} \sum_{s=-1}^{1} a_{1,s}^{(k,\ell)} T_{1,s}^{(p)} . \tag{8}$$

The scaling factors $a_{r,s}^{(k,\ell)}$ are the Fourier coefficients of the interaction-frame trajectory of the $T_{r,0}$ spherical spin-tensor operators [31]

$$\tilde{T}_{r,0}(t) = \sum_{s=-r}^{r} a_{r,s}(t) T_{r,s} = \sum_{s=-r}^{r} T_{r,s} \sum_{k=-\infty}^{\infty} \sum_{\ell=-s}^{s} a_{r,s}^{(k,\ell)} e^{i(k\omega_{\mathrm{m}} + \ell\omega_{\mathrm{eff}})t} \tag{9}$$

This manuscript was accepted by J. Chem. Phys. Click here to see the version of record.

and can be calculated analytically for ideal π pulses.[27] In the case of real, non-ideal pulses, the Fourier coefficients have to be calculated numerically from the interaction-frame trajectory. The first-order effective Hamiltonian $\bar{\mathcal{H}}^{(1)}$ is given by

$$\bar{\mathcal{H}}^{(1)} = \tilde{\mathcal{H}}_{(1)}^{(0,0,0)} + \sum_{n_0,k_0,\ell_0} \tilde{\mathcal{H}}_{(1)}^{(n_0,k_0,\ell_0)} \tag{10}$$

and the second-order effective Hamiltonian $\bar{\mathcal{H}}^{(2)}$ by

$$\bar{\mathcal{H}}^{(2)} = \tilde{\mathcal{H}}_{(2)}^{(0,0,0)} + \sum_{n_0,k_0,\ell_0} \tilde{\mathcal{H}}_{(2)}^{(n_0,k_0,\ell_0)} \tag{11}$$

with

$$\begin{aligned} \tilde{\mathcal{H}}_{(2)}^{(n_0,k_0,\ell_0)} &= \sum_{\nu,\kappa,\lambda} -\frac{1}{2}\frac{\left[\tilde{\mathcal{H}}^{(n_0-\nu,k_0-\kappa,\ell_0-\lambda)},\tilde{\mathcal{H}}^{(\nu,\kappa,\lambda)}\right]}{\nu\omega_{\mathrm{r}}+\kappa\omega_{\mathrm{m}}+\lambda\omega_{\mathrm{eff}}} \\ &= \sum_{\nu,\kappa,\lambda} -\frac{1}{2}\frac{\omega_p^{(n_0-\nu)}\omega_p^{(\nu)}}{\nu\omega_{\mathrm{r}}+\kappa\omega_{\mathrm{m}}+\lambda\omega_{\mathrm{eff}}} A_{\kappa,\lambda}(k_0,\ell_0) \end{aligned} \tag{12}$$

at the tri-modal resonance condition

$$n_0\omega_{\mathrm{r}} + k_0\omega_{\mathrm{m}} + \ell_0\omega_{\mathrm{eff}} = 0. \tag{13}$$

Here, $A_{\kappa,\lambda}(k_0,\ell_0)$ contains the spin part of the Hamiltonian (commutator terms) scaled with the Fourier coefficients $a_{r,s}^{(k_0-\kappa,l_0-\lambda)}$ and $a_{r,s}^{(\kappa,\lambda)}$. Note that the denominator in Eq. (12) cannot be zero and resonant terms must be excluded.

In theory, n_0, k_0 and ℓ_0 can be any set of integer numbers that fulfills Eq. (13) with the strength of the first-order recoupling condition given by the scaling factor $a_{r,s}^{(k,\ell)}$. For ideal pulses where the effective field is zero, one can describe the sequence in a bi-modal Floquet picture and the resonance condition of an $\mathrm{R}N_n^\nu$ sequence is given by $k_0 = -nn_0$. It can be shown that for such ideal $\mathrm{R}N_n^\nu$ sequences, the coefficients $a_{r,s}^{(k_0,0)}$ are only non zero for $k_0 = (N/2)z - s\nu$ with z being an integer that has the same parity as r.[27] This condition yields resonant first-order contributions to the Hamiltonian for $\mathrm{R}N_n^\nu$ sequences in a bi-modal

Floquet picture given by $\tilde{\mathcal{H}}^{(n_0,k_0)} = \tilde{\mathcal{H}}^{(n_0,-nn_0)}$ (see Eq. (8)). For the $\mathrm{R}26_4^{11}$ sequence relevant non-zero terms are

$$\tilde{\mathcal{H}}^{(\mp1,\pm4)} = \omega_{1,2}^{(\mp1)} a_{2,\pm2}^{(\pm4)} T_{2,\pm2}^{(1,2)} \tag{14}$$

containing only double-quantum terms. If the pulses do not correspond to an ideal inversion, we have to use the full tri-modal picture including the effective field ω_{eff}. It can be shown that for an R-type sequence, the effective field axis lies close to the z axis and that the selection rules for the ideal sequence $k_0 = (N/2)z - sv$ are still valid and $\ell_0 = -s$ has to be fulfilled simultaneously, resulting in resonant first-order contributions to the effective Hamiltonian given by $\tilde{\mathcal{H}}^{(n_0,k_0,\ell_0)} = \tilde{\mathcal{H}}^{(n_0,-nn_0,\ell_0)}$ where $\ell_0 = \pm2$ for double-quantum recoupling or $\ell_0 = 0$ for zero-quantum recoupling. For the $\mathrm{R}26_4^{11}$ sequence that selectively recouples the double-quantum terms, the relevant terms are

$$\tilde{\mathcal{H}}^{(\mp1,\pm4,\mp2)} = \omega_{1,2}^{(\mp1)} a_{2,\pm2}^{(\pm4,\mp2)} T_{2,\pm2}^{(1,2)}. \tag{15}$$

In the presence of an effective field, the resonance condition (Eq. (13)) is slightly shifted compared to the ideal case leading to the recoupling Hamiltonian as given in Eq. (15).

Besides the desired resonant contributions, we also have to discuss the non-resonant error terms that can lead to a truncation of the resonant part of the Hamiltonian. In first order, the error terms originate from a term directly proportional to the isotropic chemical-shift Hamiltonian given by

$$\tilde{\mathcal{H}}^{(0,0,0)} = \sum_{p=1}^{2} \omega_p^{(0)} \sum_{s=-1}^{1} a_{1,s}^{(0,0)} T_{1,s}^{(p)}. \tag{16}$$

Evaluation of the non-resonant second-order error terms (Eq. (12)) shows that the biggest contributions often come from the CSA-CSA cross terms. They are obtained by evaluating the commutators in Eq. (12).

This manuscript was accepted by J. Chem. Phys. Click here to see the version of record.

$$A_{\kappa,\lambda}(k_0,l_0) = \left(a_{1,-1}^{(k_0-\kappa,l_0-\lambda)}a_{1,1}^{(\kappa,\lambda)} - a_{1,1}^{(k_0-\kappa,l_0-\lambda)}a_{1,-1}^{(\kappa,\lambda)}\right)T_{1,0} + \left(a_{1,0}^{(k_0-\kappa,l_0-\lambda)}a_{1,1}^{(\kappa,\lambda)} - a_{1,1}^{(k_0-\kappa,l_0-\lambda)}a_{1,0}^{(\kappa,\lambda)}\right)T_{1,1} + \left(a_{1,-1}^{(k_0-\kappa,l_0-\lambda)}a_{1,0}^{(\kappa,\lambda)} - a_{1,0}^{(k_0-\kappa,l_0-\lambda)}a_{1,-1}^{(\kappa,\lambda)}\right)T_{1,-1}. \quad (17)$$

For the term $\widetilde{\mathcal{H}}_{(2)}^{(0,0,0)}$ it can be shown using symmetry arguments for the Fourier coefficients $a_{1,s}^{(\kappa,\lambda)}$ that $A_{\kappa,\lambda}(0,0)$ only has contributions for the $T_{1,0}$ tensor components and Eq. (17) reduces to

$$A_{\kappa,\lambda}(0,0) = \left(a_{1,-1}^{(-\kappa,-\lambda)}a_{1,1}^{(\kappa,\lambda)} - a_{1,1}^{(-\kappa,-\lambda)}a_{1,-1}^{(\kappa,\lambda)}\right)T_{1,0}. \quad (18)$$

In order to obtain the most efficient recoupling by an $\mathrm{R}N_n^\nu$ sequence, the triple-mode resonance condition (Eq. (13)) has to be fulfilled and the first-order dipolar scaling factor given in Eq. (15) has to be maximized while simultaneously minimizing the first-and second-order error terms. A similar theoretical descriptions holds true for C sequences and can be found in detail in Ref. 16 and 24. In the following we will discuss three approaches for optimizing such sequences.

Numerical Results and Discussion

The additional effective fields, as discussed above, can be caused by an error in the rf-field amplitude (missetting or inhomogeneity), pulse transients induced by the resonant circuit, or fictitious fields caused by second-order error terms. The first two sources can be seen in the numerical simulations shown in Fig. 2 where the magnitude of the effective fields is plotted for the $\mathrm{R}26_4^{11}$ sequence and a super-cycled version, denoted as SR26, as a function of the rf-field amplitude (Fig. 2A) and the magnitude of the quadrature phase transients (Fig. 2B). The influence of rf-field amplitude deviations from the theoretical value on the magnitude of the effective fields is negligible for SR26 but significant for R26. In the case of pure in-phase pulse transients (amplitude transients, ν_{off} = 0 kHz), an effective field is present for R26 as the amplitude transients induced by the time constant of the pulse leads to an altered flip angle (Eq.(1)). The amplitude transients lead to a reduced effective nutation frequency due to

This manuscript was accepted by J. Chem. Phys. Click here to see the version of record.

the finite rise time of the pulse. The reduction in the effective flip angle is partially compensated by the introduction of quadrature phase transients as they also modify the effective pulse amplitude. Nevertheless, pure in-phase amplitude transients do not generate an effective field for SR26 as the stability towards rf-field amplitude misset is fairly high for the super-cycled version and also quadrature phase transients generate only small effective fields (Fig. 2B).

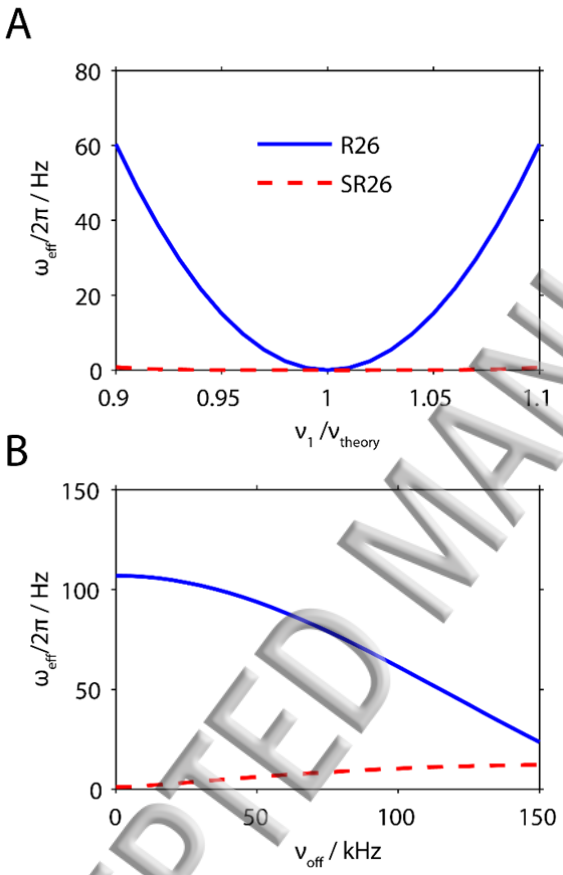

Figure 2: The effective fields after a full R*N* block for R26 (solid blue) and after a full super cycle SR26 (dashed red) as a function of the rf-field amplitude (A) and the magnitude of phase transients (B). The pulse transients were modelled with a constant rise time of 500 ns and variable electronic offset frequency (Eq.(1)).

The effective fields (from either pulse transients of rf-field amplitude errors) lead to a detuning of the resonance condition of the $\mathrm{R26}_4^{11}$ sequence resulting in a decreased transfer efficiency. There are three possible ways to optimize the transfer efficiency of the pulse

This manuscript was accepted by J. Chem. Phys. Click here to see the version of record.

sequence by counteracting the detuning caused by the effective fields: (i) asynchronous implementation of the R sequence, (ii) the use of super-cycled sequences, and (iii) implementation of pulse-transient compensated pulses. All three possible approaches to optimize the pulse sequence are explored in the numerical simulations of Fig. 3. An experimentally straight-forward way to compensate the impact of effective fields in symmetry-based recoupling sequences is the breaking of the rotor synchronization of the pulse sequence to match the modified resonance condition of Eq. (13). The simplest way to achieve this is by a change of the MAS frequency resulting in an asynchronous sequence. Numerical simulations of the transfer efficiency as a function of the MAS frequency and the rf-field amplitude are shown in Fig. 3A for R26 and Fig. 3B for SR26. The simulations were

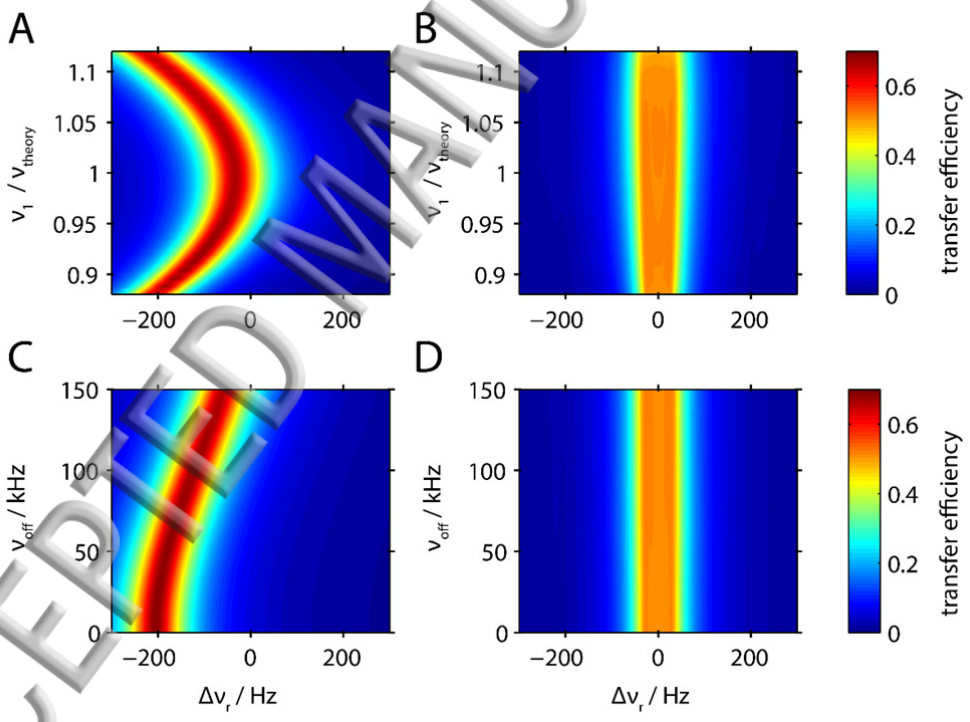

performed for parameters similar to the model compound of doubly ^{13}C-labeled diammonium phthalate with ^{13}C-labels at the two carbonyl groups. This substance poses a challenge for recoupling sequences due to a rather large CSA tensor (δ = 77 ppm and η = 0.68) and an intermediate dipolar coupling of $\nu_{1,2}$ = 585 Hz.[32]

Figure 3: Numerical simulation of double-quantum transfer efficiency as a function of the change of the MAS frequency and the rf-amplitude and the magnitude of the phase transients, respectively. The simulations were performed with a dipolar coupling of 585 Hz and a chemical-shift anisotropy of 8.75 kHz. The ideal rf-amplitude ν_1 corresponds to a value of 62.5 kHz at a MAS frequency of 9.615 kHz. A) Transfer efficiency for R26 with ideal rectangular pulses, B) SR26 with ideal rectangular pulses, C) R26 with pulse transients (τ_{rise}= 500 ns, variable ν_{off}) at the ideal rf-amplitude ν_1 = 62.5 kHz. D) SR26 using the same parameters for the pulse transients.

Figure 3A shows that even for a perfect inversion propagator, corresponding to an rf-field strength of 62.5 kHz, there is an effective field for the R26 sequence of 32 Hz which originates from the second-order contributions of the CSA tensor and scales roughly quadratic with the CSA tensor (see Supporting Information). Optimum recoupling is achieved by changing the MAS frequency by the same amount. The total value of the effective field is determined by a superposition of the contributions by the second-order cross terms and by the altered effective flip angle of the pulses. The simulations show that, despite the increasing magnitude of the effective field, almost maximum polarization transfer can be achieved over the whole range of rf-field amplitudes by compensating the effective field through a change in the MAS frequency. There are many more potential error terms, which have been neglected in this description based on the assumption that the CSA terms are dominating in our case. There are, for example, also heteronuclear dipole/dipole cross terms if the recoupling is done without decoupling. They can be significant for protonated carbons due to the large magnitude of the heteronuclear dipolar coupling of directly bound spin pairs. In the Supporting Information, Fig. S2, we show simulations to illustrate the effective fields generated by heteronuclear dipolar couplings. Under cw proton decoupling, these effective fields still exist but are significantly reduced in magnitude.

A second approach is the application of a super-cycled version of the R sequence. The sequence SR26[20,21] represents such an implementation which successfully mitigates the impact of an effective field by removing second- and some of the higher-order cross terms (Fig. 3B). This can be seen from the maximum of the transfer efficiency for perfect inversion

This manuscript was accepted by J. Chem. Phys. Click here to see the version of record.

pulses at an rf-field strength of 62.5 kHz which is the theoretical value for the applied MAS frequency. The super-cycled SR26 sequence also compensates rf-field amplitude missetting (Fig. 3B) but at the cost of losing the γ encoding of the sequence under MAS. Therefore, the maximum transfer efficiency for SR26 is 52%, whereas the maximum transfer for R26 is 73%.

Adding analytically modelled pulse transients to the simulations (Fig. 3C and 3D) results in a further shift from the theoretical recoupling condition for the R26 sequence. The pulse transients were simulated according to the model given in Eq. (1).[11] A time constant of τ_{rise} = 500 ns and a variable offset frequency ν_{off}, corresponding to experimentally observed pulse parameters, were used for the simulations. An additional effective field due to the quadrature component of the pulse transients is superimposed on the effective field observed using ideal rectangular pulses. The best result is observed for high phase transients as the amplitude transient deteriorates the effective flip angle which is partially compensated by the introduction of phase transients. Analogous calculations for the super cycle SR26 show that pulse transients are compensated almost perfectly (Fig. 3D).

Effective fields generated by a missetting of the rf-field amplitude or the pulse transients can directly be influenced by the experimentalist while effective fields generated by second-order cross terms are largely determined by the spin system. As discussed above, CSA-CSA cross terms are the main source of such effective fields. Their magnitude is shown in Figure 4A as a function of the applied rf field and the detuning of the MAS frequency. The cross terms were calculated according to Eqs. (12) and (18). The magnitude of the terms is virtually unaffected by the MAS frequency but scales nearly linearly with increasing rf-field amplitude. Note that the Fourier coefficients in Eq. (18) are almost independent of the MAS frequency. For a given rf field the MAS frequency changes the second-order Hamiltonian only through the denominator in Eq. (12). The magnitude of the effective fields caused by CSA cross terms and the rf-field amplitude missetting matches the detuning of the MAS frequency obtained by numerical simulations very well (Fig. 4B). Analogous calculations for the super

This manuscript was accepted by J. Chem. Phys. Click here to see the version of record.

cycle SR26 yield cross terms that are five orders of magnitude smaller and the effective field due to these cross terms can be neglected to very good approximation.

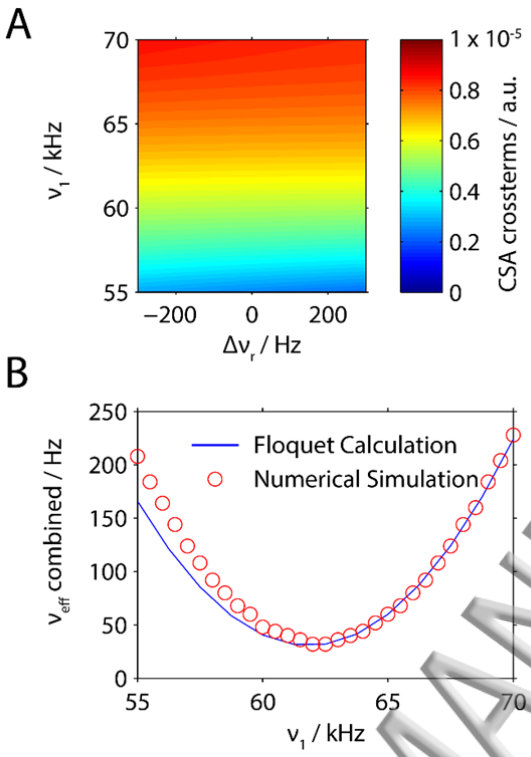

Figure 4: A) The magnitude of the second-order CSA-CSA scaling coefficients for R26-recoupling calculated with ideal rectangular pulses as a function of the MAS detuning and the rf-amplitude ν_1 at an MAS frequency of 9.615 kHz. For the fictitious effective fields, these terms are scaled with the coefficients $\omega_p^{(\nu)}$ and $\omega_p^{(n_0-\nu)}$ to match the detuning of 32 Hz at an ideal rf-field amplitude. B) The fictitious fields from error terms added to the effective field caused by the altered flip angle calculated by interaction-frame transformation (blue line). The combined effective field agrees with the MAS detuning obtained from numerical simulations (red dots, taken from Figure 3A).

Numerical simulations and a triple-mode Floquet description of the R26 sequence give insight on the contributions to the effective field after one modulation period. The most important contributions are the rf-amplitude misset that results in effective fields of up to 60 Hz for a misset of 10% and pulse transients that add an additional field between 20 and 100 Hz depending on the magnitude of the amplitude and phase transients. A third contribution observed in the numerical simulations is due to the second-order CSA-CSA

cross terms. The magnitude of the generated fictitious field depends mainly on the spin system.[33] It was calculated to be 32 Hz for a CSA tensor of 8.75 kHz.

Experimental Results and Discussion

In order to verify the results from numerical simulations, we have experimentally optimized the polarization transfer using the three discussed approaches. Diammonium phthalate selectively labelled at the carbonyl groups and diluted 1:7 in natural abundance served as a model compound. Polarization-transfer curves were measured at a static magnetic field of B_0 = 7.1 T corresponding to a situation with a relatively small CSA tensor (5.25 kHz). In addition, measurements at a static magnetic field of 16.6 T were carried out where the influence of the CSA tensor is much more important.

To simulate different experimental conditions, we ran the experiments with three different cable lengths between the preamplifier and the probe (setup 1-3, 125 cm, 155 cm, and 170 cm cable length). The cable length changes the impedance of the resonance circuit if any of the electrical components is not perfectly matched. The change of impedance results in an alteration of the pulse amplitude and phase. These differences can be seen in Fig. 5A where the B_1-field shapes measured in the probe by a pickup coil[12] are plotted for a basic $R_\varphi R_{-\varphi}$ element. The B_1 shapes seen by the sample differ from each other at the pulse discontinuities, strongly affecting the transfer efficiency as can be seen in Fig. 5B where the transfer efficiency is plotted as a function of the mixing time and the rf-field amplitude. Only in setup 1 significant polarization transfer could be achieved (38%). In both the setups 2 and 3 less than 12% efficiency was measured. Use of compensated pulses (bottom row in Fig. 5B) results in a high reproducibility of the polarization-transfer condition and also higher polarization-transfer efficiencies of 36-42%. The recoupling condition for transient-compensated pulses becomes predictable because the effective fields caused by pulse transients are suppressed. The compensation of pulses leads to an almost perfect recovery of an inversion propagator for the basic R element without residual effective fields after the rotation.

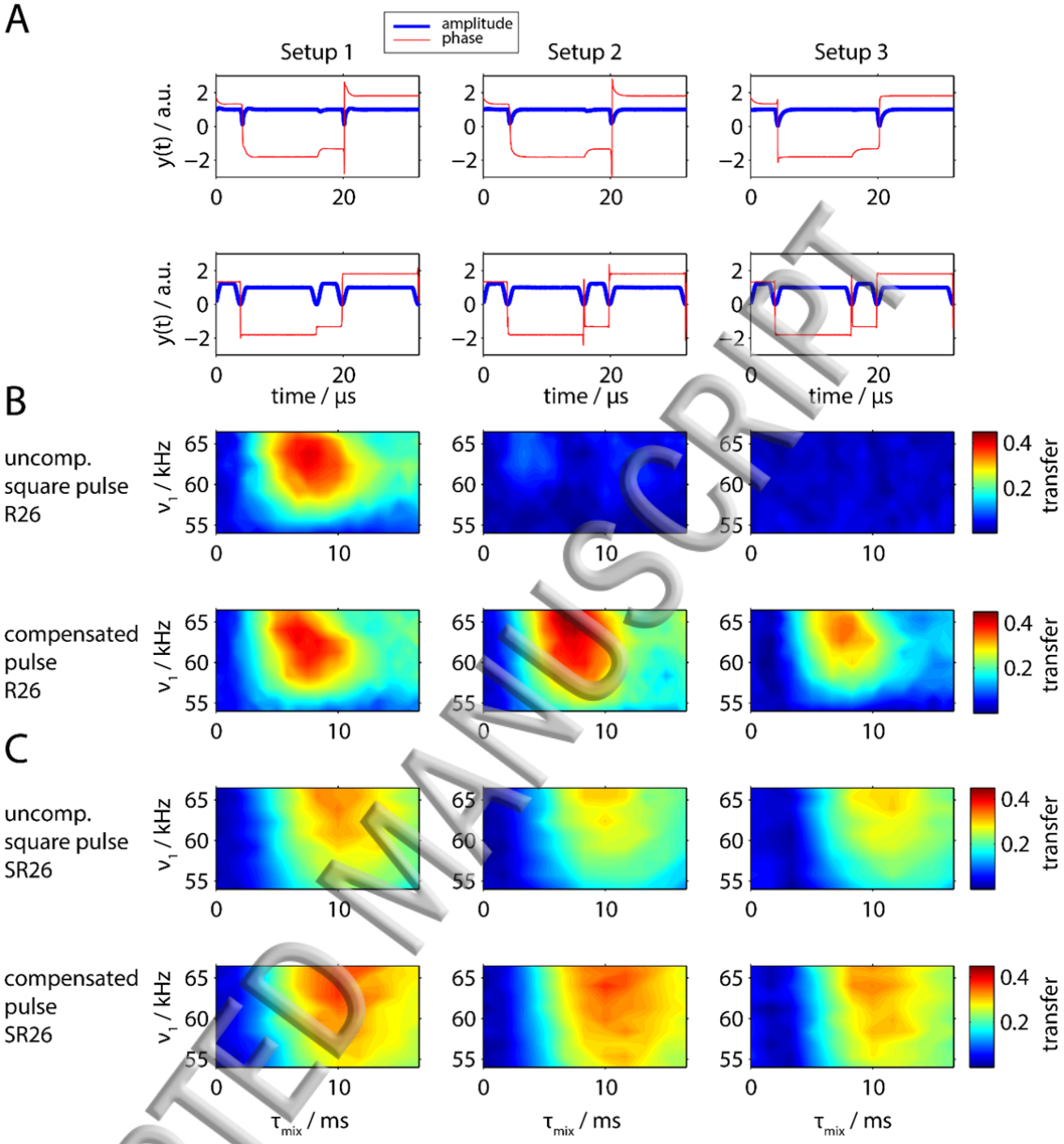

Figure 5: Experimental double-quantum transfer efficiency for R26 recoupling at 9.615 kHz MAS in doubly ^{13}C labelled phthalate. The external magnetic field was 7.1 T, with a basic R-element $(\pi/2)_{\varphi}(3\pi/2)_{\varphi+\pi}$. Decoupling during the R sequence was implemented using cw irradiation with a rf-field amplitude of 105 kHz. A). Measured B_1-shapes for conventional hard pulses (top row) and the compensated pulses (bottom row). B) Transfer efficiency for three different setups (125 cm, 155 cm, and 170 cm cable length) for square pulses (top row) and compensated, amplitude-shaped pulses with flip-angle correction (bottom row). C) Analogous measurements as in B) with the super cycle SR26.

It is interesting to observe that setup 3, which has the smallest quadrature component, shows the worst recoupling performance which agrees with the calculations shown in Fig. 2B. It is nearly impossible to predict the recoupling performance a priori solely based on the shape of the pulse transients. It is by chance that setup 1 showed favorable recoupling conditions. The maximum transfer could potentially be further optimized by higher decoupling power and a reduction of the B_1-field inhomogeneity (restricted sample). Decoupling efficiency becomes more important for carbons with directly bound protons.

The second possible approach is the use of the super-cycled SR26 sequence which partially compensates effective fields at the cost of a lower theoretical transfer efficiency. Figure 5C shows the transfer efficiency for the SR26 pulse sequence using rectangular pulses and transient-compensated pulses. One can clearly see a significant improvement compared to the transfer efficiency under the uncompensated R26 sequence (Fig. 5B) and transfer efficiencies around 29% are achieved. However, the transfer efficiency of SR26 can still be improved to roughly 34% using transient-compensated pulses as can be seen in the bottom row of Fig. 5C. The SR26 sequence shows clearly a weaker dependence for the transfer on the rf-field amplitude but the transfer efficiencies are significantly lower than in the transient-compensated R26 sequence. This is due to the loss of γ encoding in the SR26 sequence, which leads to a reduction in the theoretical transfer efficiency. For the highest transfer efficiency, transient-compensated pulses are clearly the better solution even if they currently require specialized equipment.

Transient compensation has not yet been implemented on commercial spectrometers and, therefore, can only be performed on a spectrometer after modification of the probe with a pick-up coil. If transient compensation is not possible, asynchronous sequences for compensating the effective field or super-cycled sequences are an alternative that can be used. The asynchronous implementation of the R26 sequence was first investigated at low static field (7.1 T), and hence, for a small magnitude of the second-order CSA cross terms. In order to implement asynchronous conditions for the sequence, the MAS frequency was

This manuscript was accepted by J. Chem. Phys. Click here to see the version of record.

varied in steps of 10 Hz from +100 to -100 Hz with respect to the synchronous spinning frequency of 9.615 kHz. In addition, the rf-field amplitude was varied independently in order to show the effect of an altered effective flip angle. Even for the setup 1 (Fig. 5) with favorable pulse transients the transfer efficiency can be improved by 6% to 44% by satisfying the asynchronous condition as shown in Fig. 6.

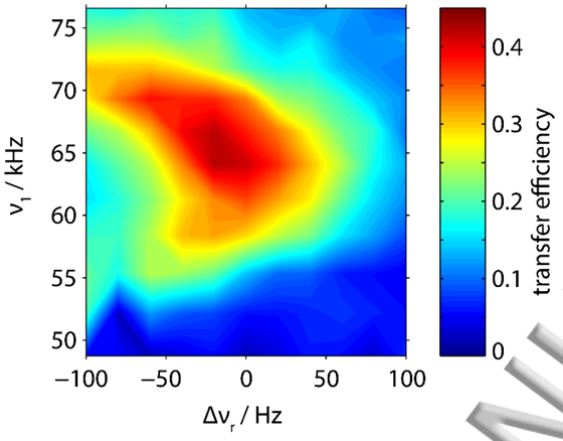

Figure 6: The experimental double-quantum transfer efficiency for ammonium phthalate as a function of the MAS frequency detuning and the rf-field amplitude. The theoretical rf-field amplitude is 62.5 kHz with a synchronous MAS frequency of 9.615 kHz. The experiments were performed on a 7.1 T magnet with a 125 cm cable, corresponding to the setup 1 in Fig. 5. The superposition of the effective field generated by the CSA cross terms is obvious as the optimal MAS frequency at the recoupling condition is shifted by -20 Hz from the one determined from the symmetry condition.

In actual NMR applications, measurements are usually performed at high fields for optimum sensitivity and spectral resolution. We therefore compare the performance of each implementation at a higher static field (16.6 T) with larger second-order CSA contributions and without prior knowledge of the actual B_1 shapes, i.e., the pulse transients. Asynchronous implementation was tested by changing the MAS frequency in order to compensate for the combined effective fields from the CSA-CSA cross terms and the pulse transients. The MAS frequency was varied from 9.615 (synchronous), to 9.565, and 9.515 kHz while keeping the mixing time fixed at the experimentally optimized value. The highest observed transfer efficiency of 48% for R26 was found at a MAS detuning of -100 Hz (Fig. 7A) compared to an

efficiency of 24% for the synchronous version. For SR26 the highest transfer efficiency of 38% was found for the synchronous implementation (Fig. 7B) and detuning resulted in significantly lower polarization transfer. The super-cycled sequence suppresses the effective fields very efficiently and can be implemented without experimental optimization. This is achieved, however, at the price of a lower transfer efficiency. Without the knowledge of the pulse transients and the magnitude of the CSA tensor, estimation of the required MAS detuning is not feasible. The optimization of the asynchronous recoupling condition by changing the MAS frequency has to be done experimentally and can be tedious especially for samples with low signal-to-noise ratio. As demonstrated in Fig. 7, however even a quick scan of the MAS frequency can restore transfer efficiencies for R26, to a value that is higher than the ones obtained for synchronous SR26 if the sample yields decent signal intensities.

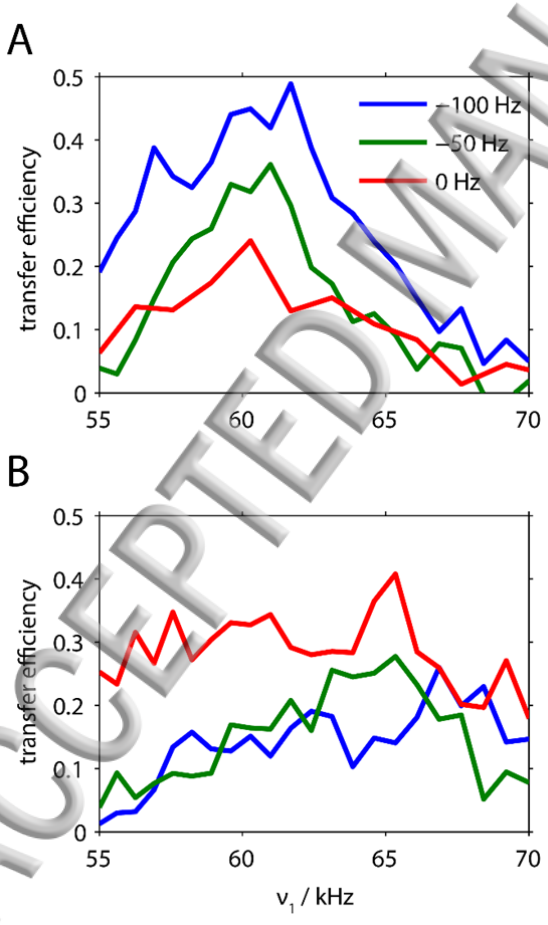

Figure 7: Experimental transfer for synchronous and asynchronous implementation of R26 (A) and SR26 (B), using conventional square pulses at a static magnetic field of 16.6 T. The advantages of the

This manuscript was accepted by J. Chem. Phys. Click here to see the version of record.

R26 sequence are the higher transfer efficiency for the asynchronous implementation as compared to SR26 due to γ-encoding. The advantages of SR26 are the robustness towards second-order error-terms and rf-field missetting, making an asynchronous implementation obsolete. The maximum transfer for R26 is 48%, whereas the maximum of SR26 corresponds to 38%, as reported in the literature.[20]

Materials and Methods

Numerical simulations were performed using the GAMMA spin-simulation environment.[34] Different crystallites were simulated with 300 ZCW orientations for powder averaging.[35] The MAS frequency was set to 9.615 kHz for all the simulations and analytical calculations. All experiments presented were performed at the same MAS frequency, unless stated otherwise. Orientations of dipole-dipole and chemical shift tensors were taken from quantum-mechanical calculations based on the crystal structure of diammonium phthalate.[32]

The interaction-frame transformation in the Floquet calculation was done numerically in MATLAB using a discrete time-step of 50 ns. Eq. (6) was discretized and it was assumed that the rf-field phase and amplitude were constant during the time steps. The Fourier coefficients describing the scaling factors and error terms were calculated by Fourier transform after transformation into a second rotating frame with the effective field. Finally, a conversion from Cartesian to a spherical-tensor representation was performed.

Phthalic acid-α,α-$^{13}C_2$ was purchased from Isotec. A mixture of unlabeled and labeled sample with a ratio of 7:1 was prepared. For the synthesis of the diammonium salt, an excess of aqueous ammonia was added and the product was crystallized and purified by lyophilisation. The experiments on the 7.1 T magnet (300 MHz proton resonance frequency) were carried out on a Bruker Avance III HD spectrometer using a 1.9 mm double-resonance Bruker probe. The experiments on the 16.6 T magnet (600 MHz proton resonance frequency) were carried out on a Bruker Avance III spectrometer using a 2.5 mm triple-resonance Bruker probe. Both rotors were completely filled without sample restriction. Processing was done in Topspin (Bruker Biospin, Rheinstetten, Germany) and zeroth- and first-order phase corrections were

This manuscript was accepted by J. Chem. Phys. Click here to see the version of record.

imposed manually after Fourier transformation. The transfer efficiency was calculated by referencing the build-up peak to the source peak at zero mixing time. The transient compensation was performed as described in Ref. [12].

Conclusions

In symmetry-based R sequences unwanted effective fields are important sources of decreased transfer efficiency when measuring intermediate or small couplings because they lead to a mismatch of the two-frequency resonance condition. The sources of the effective fields can be second-order CSA-CSA cross terms, pulse transients, or a radio-frequency field that does not generate the required flip angle. The latter can be due to a missetting of the rf-field amplitude or due to rf-field inhomogeneity. There are three strategies to compensate the effective fields and restore efficient polarization transfer: (i) asynchronous recoupling by detuning the spinning frequency, (ii) super-cycled R sequences, and (iii) transient-compensated pulses. Each of the three methods has different advantages and disadvantages. The asynchronous recoupling by a change of the MAS frequency can compensate all the three sources of effective fields and leads to the highest transfer efficiencies but needs experimental optimization. The super-cycled sequences have generally lower efficiencies due to the lack of γ encoding but they compensate for all the three sources and do not need any optimization. Transient compensation can be implemented without experimental optimization and makes the performance of the sequences very reproducible but compensate only effective fields originating from pulse transients.

The choice of use of which method or combination of methods to optimize the transfer efficiency depends on the capabilities of the spectrometer and the relative magnitude of the the three different contributions. On spectrometers with the capability of phase-transient compensation, transient-compensated pulses possibly in combination with an asynchronous implementation to compensate for the second-order terms leads to the best results. On spectrometers without the possibility to do transient compensations, an asynchronous

implementation is the way to go if the S/N allows optimization of the spinning frequency. Otherwise super-cycled sequences offer the best chance to obtain reasonable transfer efficiencies without the need for experimental optimization.

Because the best transfer efficiency requires transient compensation, it is hoped that this capability will soon be provided by the spectrometer manufactures to make the method more generally applicable.

Supplementary Material

The supplementary data contains additional figures showing calculations of the Fourier coefficients for the R26 sequence, plots showing the influence of other second-order cross terms besides CSA-CSA, plots of the measured experimental phase transients, and the simulation code used in the paper.

Acknowledgments

The authors want to thank Dr. Kazuyuki Takeda for valuable inputs on the transient compensation, Dr. Anders Bodholt Nielsen for sharing preliminary results on the Floquet description in the second interaction frame, and Nino Wili for stimulating discussions. Alexander Däpp is acknowledged for the technical support. This work was supported by the Swiss National Science Foundation (grants 200020_146757 and 200020_159797), the ETH Zurich (grant ETH-10 15-1) and a PEP grant from the Indo-Swiss Joint Research Program (ISJRP).

References

[1] M. Mehring, *Principles of High Resolution NMR in Solids* ((Berlin ; New York : Springer-Verlag, 1983).

[2] M.J. Duer, *Solid State NMR Spectroscopy: Principles and Applications* (Wiley-Blackwell, 2007).

[3] A.E. Bennett, R.G. Griffin, and S. Vega, *Recoupling of Homo-and Heteronuclear Dipolar Interactions*

in Rotating Solids (NMR Basic Principles and Progress, 1994), pp. 3–77.

[4] S. Dusold and A. Sebald, Ann. Rep. NMR Spectr. 41, 185 (2000).

[5] V. Ladizhansky, Solid State Nucl. Magn. Reson. **36**, 119 (2009).

[6] N.C. Nielsen, L.A. Strassø, and A.B. Nielsen, Top. Curr. Chem. **306**, 1 (2012).

[7] K. Schmidt-Rohr, Macromolecules **29**, 3975 (1996).

[8] B. Reif, M. Hennig, and C. Griesinger, Science **276**, 1230 (1997).

[9] M.H. Levitt, in *Encycl. Magn. Reson.* (2007), pp. 165–196.

[10] M. Carravetta, M. Edén, O.G. Johannessen, H. Luthman, P.J. Verdegem, J. Lugtenburg, A. Sebald, and M.H. Levitt, J. Am. Chem. Soc. **123**, 10628 (2001).

[11] M. Mehring and J.S. Waugh, Rev. Sci. Instrum. **43**, 649 (1972).

[12] J.J. Wittmann, V. Mertens, K. Takeda, B.H. Meier, and M. Ernst, J. Magn. Reson. **263**, 7 (2016).

[13] R.W. Vaughan, D.D. Elleman, L.M. Stacey, W.K. Rhim, and J.W. Lee, Rev. Sci. Instrum. **43**, 1356 (1972).

[14] W.-K. Rhim, D.D. Elleman, and R.W. Vaughan, J. Chem. Phys. **59**, 3740 (1973).

[15] D.P. Burum, M. Under, and R.R. Ernst, J. Magn. Reson. **43**, 463 (1981).

[16] J. Weber, M. Seemann, and J. Schmedt Auf Der Günne, Solid State Nucl. Magn. Reson. **43–44**, 42 (2012).

[17] K. Takeda, Y. Tabuchi, M. Negoro, and M. Kitagawa, J. Magn. Reson. **197**, 242 (2009).

[18] Y. Tabuchi, M. Negoro, K. Takeda, and M. Kitagawa, J. Magn. Reson. **204**, 327 (2010).

[19] J.J. Wittmann, K. Takeda, B.H. Meier, and M. Ernst, Angew. Chemie - Int. Ed. **54**, 12592 (2015).

[20] P.E. Kristiansen, M. Carravetta, W.C. Lai, and M.H. Levitt, Chem. Phys. Lett. **390**, 1 (2004).

[21] P.E. Kristiansen, M. Carravetta, J.D. van Beek, W.C. Lai, and M.H. Levitt, J. Chem. Phys. **124**, 234510 (2006).

[22] G. Teymoori, B. Pahari, and M. Edén, J. Magn. Reson. **261**, 205 (2015).

[23] M. Bechmann, J. Clark, and A. Sebald, J. Magn. Reson. **228**, 66 (2013).

[24] K.O. Tan, M. Rajeswari, P.K. Madhu, and M. Ernst, J. Chem. Phys. **142**, (2015).

[25] M.H. Levitt, J. Chem. Phys. **128**, (2008).

[26] J.H. Shirley, Phys. Rev. **138**, (1965).

[27] E. Vinogradov, P.K. Madhu, and S. Vega, Top. Curr. Chem. **246**, 33 (2004).

[28] I. Scholz, J.D. Van Beek, and M. Ernst, Solid State Nucl. Magn. Reson. **37**, 39 (2010).

[29] I. Scholz, B.H. Meier, and M. Ernst, J. Chem. Phys. **127**, (2007).

[30] F.J. Dyson, Phys. Rev. **75**, 486 (1949).

[31] I. Scholz, P. Hodgkinson, B.H. Meier, and M. Ernst, J. Chem. Phys. **130**, (2009).

[32] R.A. Smith, Acta Crystallogr. Sect. B Struct. Crystallogr. Cryst. Chem. **31**, 1773 (1975).

[33] G. De Paëpe, J.R. Lewandowski, A. Loquet, A. Böckmann, and R.G. Griffin, J. Chem. Phys. **129**, (2008).

[34] S.A. Smith, T.O. Levante, B.H. Meier, and R.R. Ernst, J. Magn. Reson. Ser. A **106**, 75 (1994).

[35] V.B. Cheng, H.H. Suzukawa, and M. Wolfsberg, J. Chem. Phys. **59**, 3992 (1973).

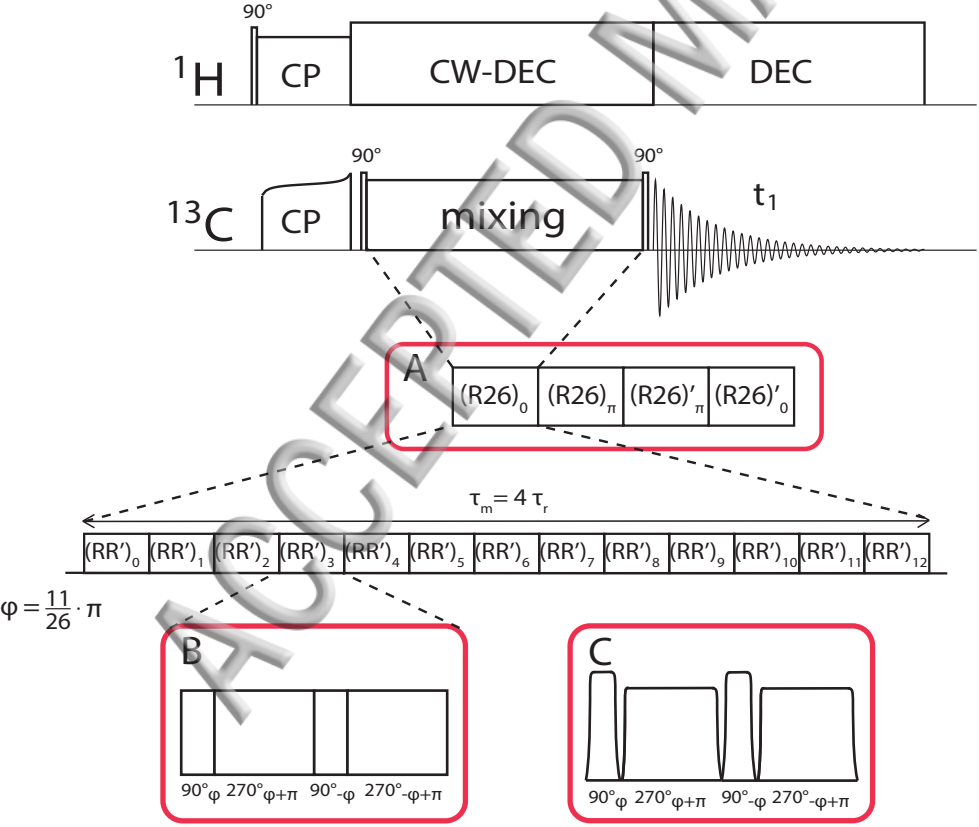
90°
^{1}H
CP
CW-DEC
DEC
90°
90°
^{13}C
CP
mixing
t_1
A
$(R26)_0$
$(R26)_\pi$
$(R26)'_\pi$
$(R26)'_0$
$\tau_m = 4\,\tau_r$
$(RR')_0$ $(RR')_1$ $(RR')_2$ $(RR')_3$ $(RR')_4$ $(RR')_5$ $(RR')_6$ $(RR')_7$ $(RR')_8$ $(RR')_9$ $(RR')_{10}$ $(RR')_{11}$ $(RR')_{12}$
$\varphi = \frac{11}{26} \cdot \pi$
B
90°φ 270°φ+π 90°-φ 270°-φ+π
C
90°φ 270°φ+π 90°-φ 270°-φ+π

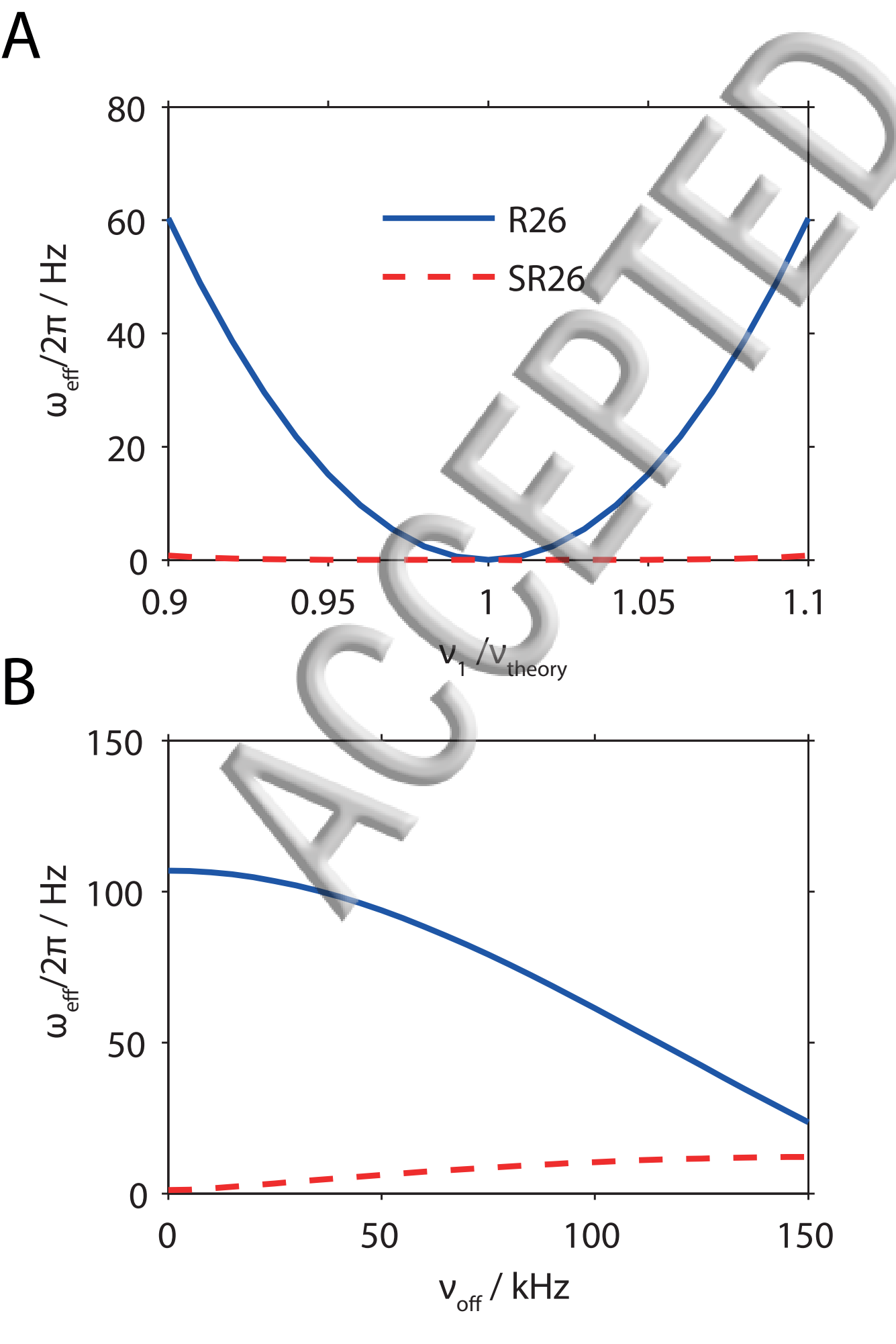
A
80
60
40
20
0
$\omega_{eff}/2\pi$ / Hz
R26
SR26
0.9
0.95
1
1.05
1.1
ν_1/ν_{theory}
B
150
100
50
0
$\omega_{eff}/2\pi$ / Hz
0
50
100
150
ν_{off} / kHz

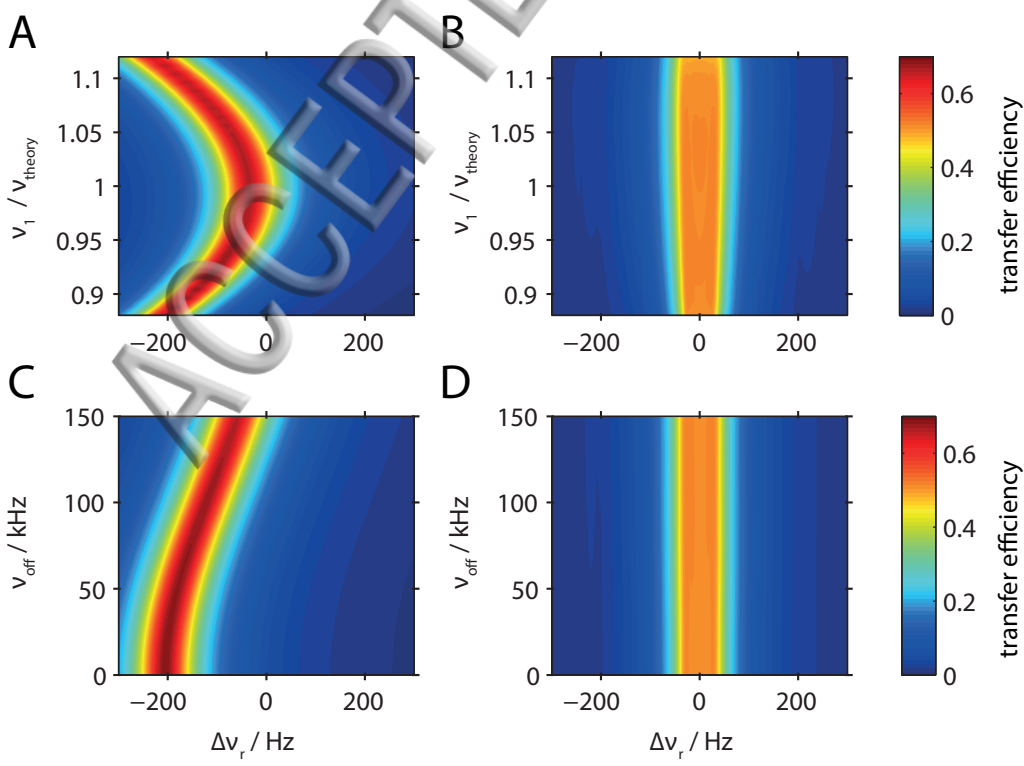
A
B
C
D
ν_1 / ν_{theory}
1.1
1.05
1
0.95
0.9
−200
0
200
ν_{off} / kHz
150
100
50
0
$\Delta\nu_r$ / Hz
transfer efficiency
0.6
0.4
0.2
0

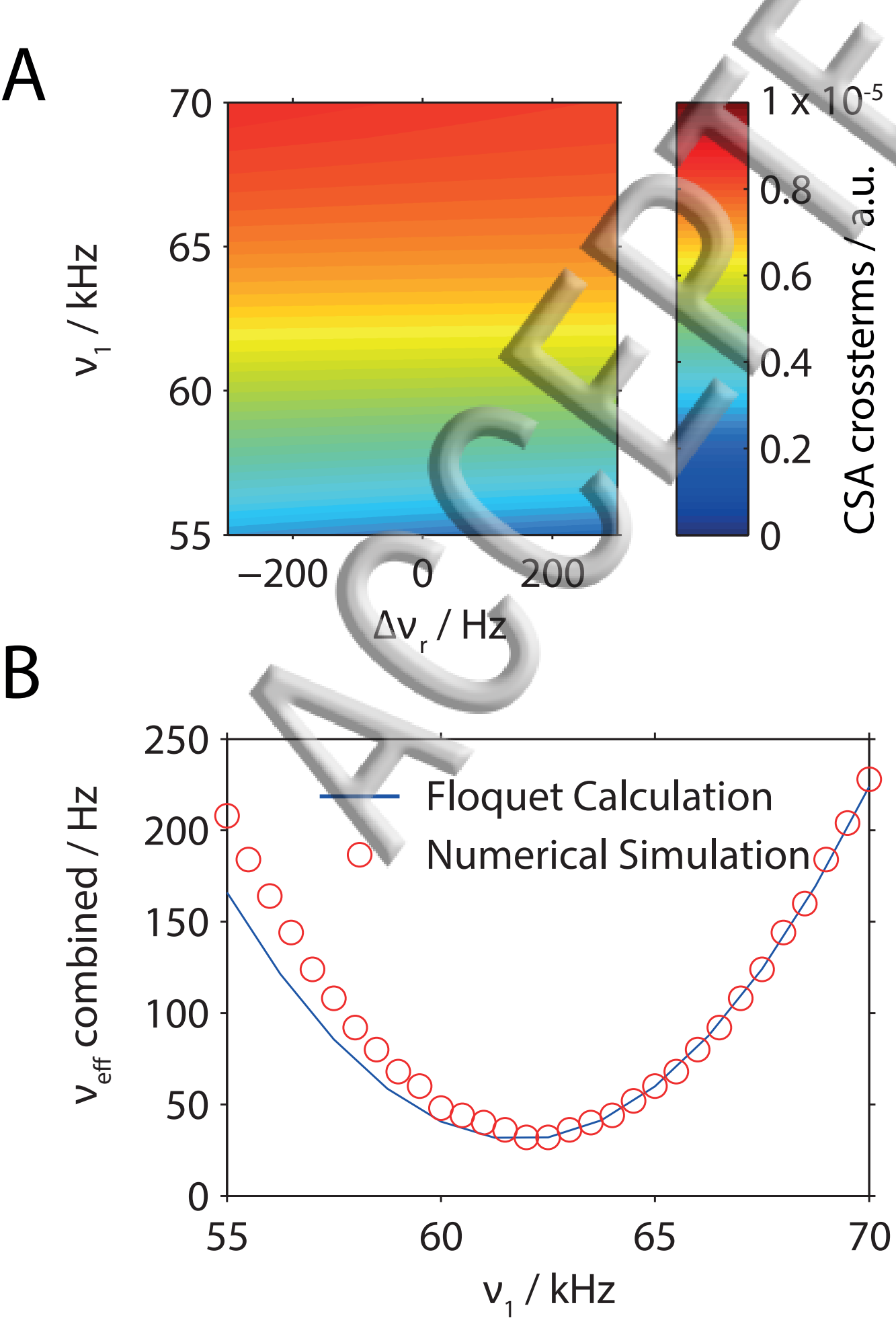
A
70
65
60
55
ν_1 / kHz
−200
0
200
$\Delta\nu_r$ / Hz
1 x 10^{-5}
0.8
0.6
0.4
0.2
0
CSA crossterms / a.u.
B
250
200
150
100
50
0
ν_{eff} combined / Hz
Floquet Calculation
Numerical Simulation
55
60
65
70
ν_1 / kHz

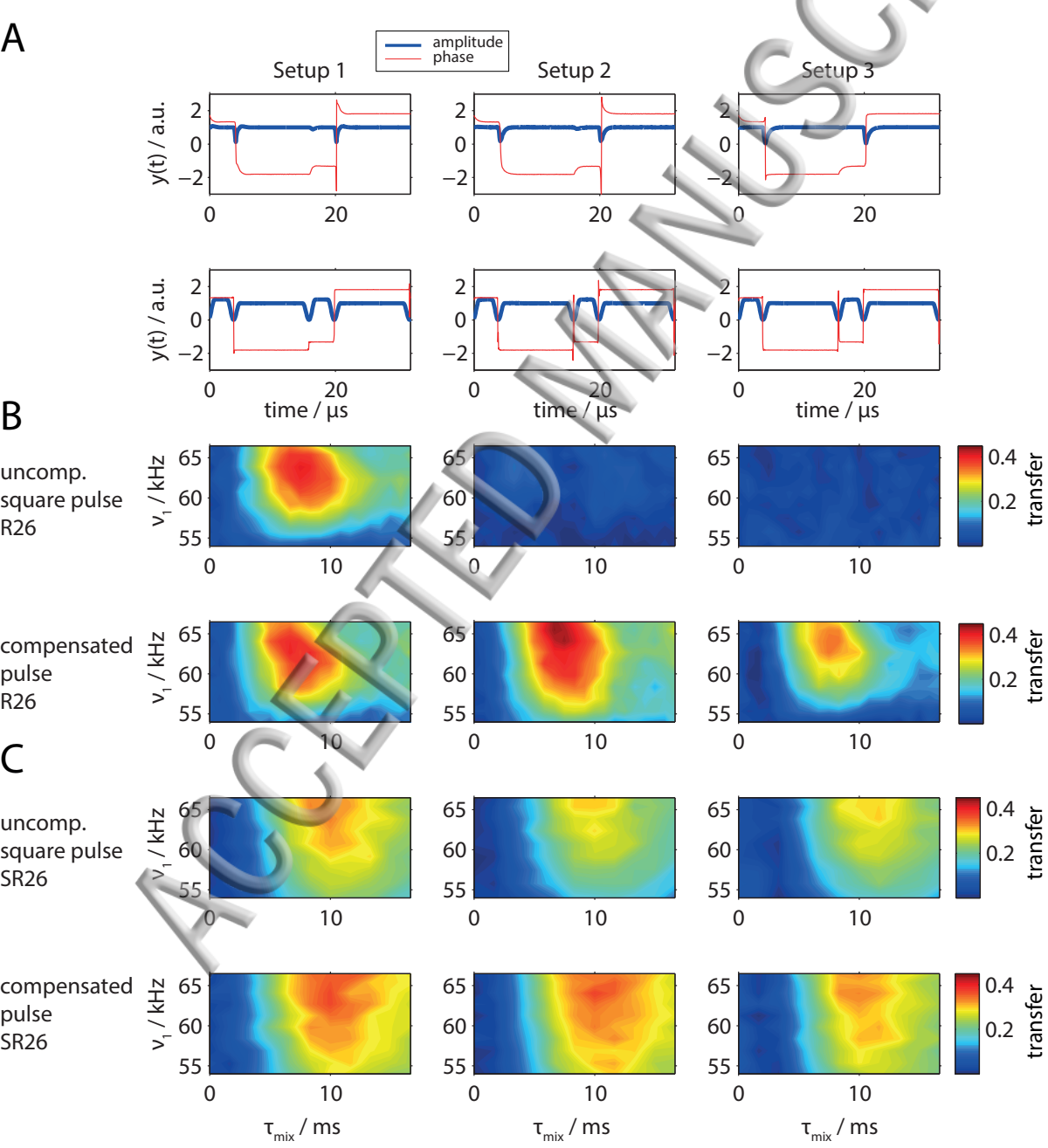

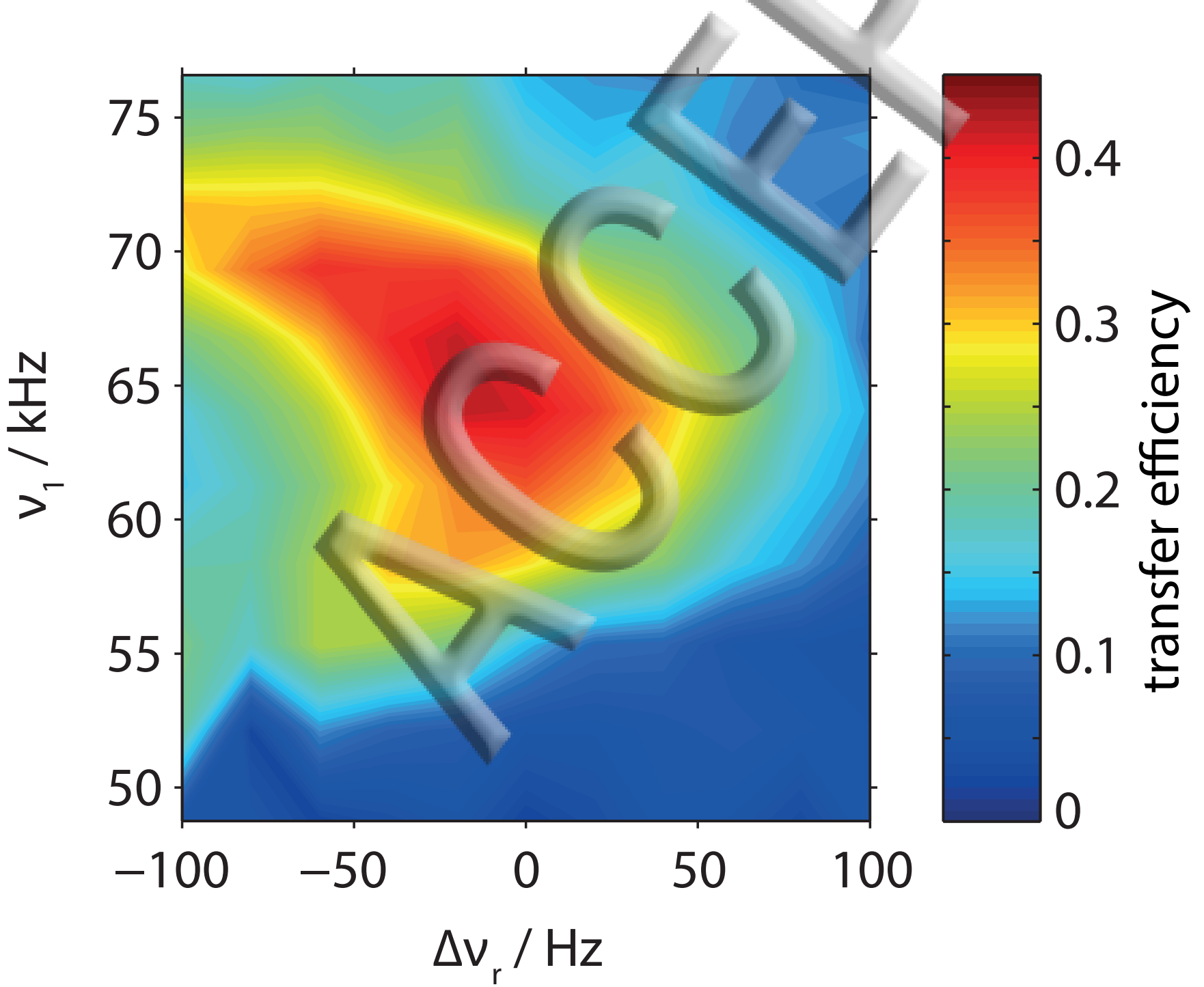
75
70
65
60
55
50
ν_1 / kHz
−100
−50
0
50
100
$\Delta\nu_r$ / Hz
0.4
0.3
0.2
0.1
0
transfer efficiency
ACCEPTED

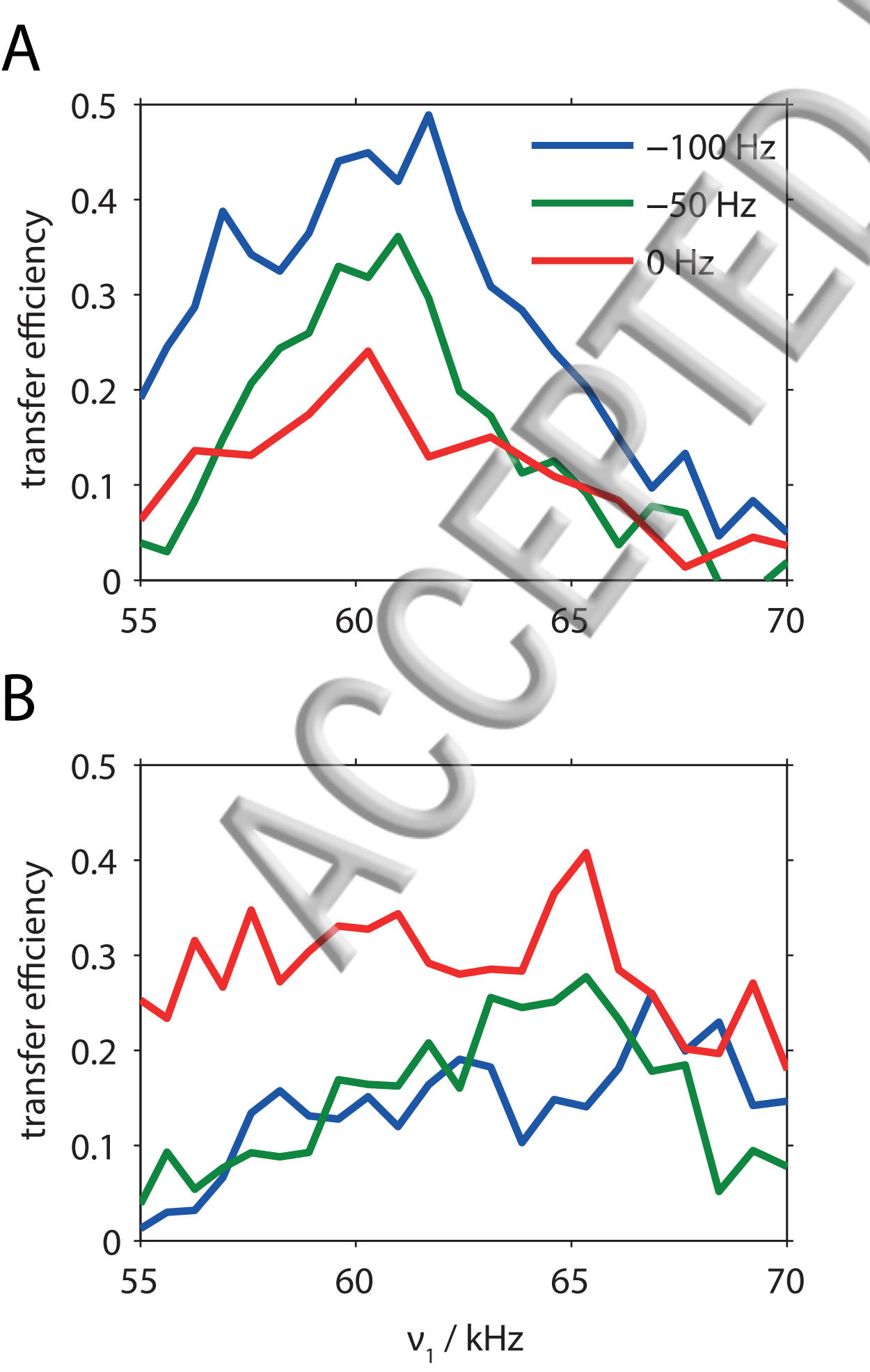
A
B
transfer efficiency
0.5
0.4
0.3
0.2
0.1
0
55
60
65
70
−100 Hz
−50 Hz
0 Hz
ν1 / kHz